

ARTICLE

<https://doi.org/10.1038/s41467-022-29601-0>

OPEN

Deforestation-induced climate change reduces carbon storage in remaining tropical forests

Yue Li¹✉, Paulo M. Brando¹, Douglas C. Morton², David M. Lawrence³, Hui Yang⁴ & James T. Randerson¹

Biophysical effects from deforestation have the potential to amplify carbon losses but are often neglected in carbon accounting systems. Here we use both Earth system model simulations and satellite-derived estimates of aboveground biomass to assess losses of vegetation carbon caused by the influence of tropical deforestation on regional climate across different continents. In the Amazon, warming and drying arising from deforestation result in an additional $5.1 \pm 3.7\%$ loss of aboveground biomass. Biophysical effects also amplify carbon losses in the Congo ($3.8 \pm 2.5\%$) but do not lead to significant additional carbon losses in tropical Asia due to its high levels of annual mean precipitation. These findings indicate that tropical forests may be undervalued in carbon accounting systems that neglect climate feedbacks from surface biophysical changes and that the positive carbon-climate feedback from deforestation-driven climate change is higher than the feedback originating from fossil fuel emissions.

¹Department of Earth System Science, University of California, Irvine, CA, USA. ²Biospheric Sciences Laboratory, NASA Goddard Space Flight Center, Greenbelt, MD, USA. ³National Center for Atmospheric Research, Boulder, CO, USA. ⁴Department of Biogeochemical Integration, Max Planck Institute for Biogeochemistry, Jena, Germany. ✉email: yue.li@uci.edu

Tropical forests store more than 200 Pg C in aboveground live biomass^{1–3}. Climate warming has the potential to contribute to a positive feedback that causes tropical forests to lose carbon, making it more difficult to stabilize the Earth's climate^{4,5}. Over the past several centuries, the expansion of agriculture in tropical regions has contributed to widespread losses of tropical forest on multiple continents^{6–8}. The rate of tropical forest loss accelerated in the 1970s (e.g., refs. ^{9,10}), and by the 1990s, direct carbon emissions from tropical deforestation were at record high levels, with estimates ranging between 0.8 and 2.2 Pg C yr^{−1} (refs. ^{11,12}). Since the 2000s, rates of tropical deforestation have slowed, contributing to an overall decline in the global carbon flux from land-use change (e.g., from 1.9 Pg C yr^{−1} in 1997 to 1.0 Pg C yr^{−1} during 2010–2019, ref. ^{11,13}). Many tropical forests continue to lose carbon in hot-spot regions¹⁴, however, as a consequence of increasing impacts from fire and other drivers of forest degradation^{15,16}. Altogether, cumulative carbon emissions from tropical deforestation and other land-cover changes in the tropics over the past several centuries are comparable to the current aboveground vegetation carbon stock¹⁷.

Apart from contributing to the build-up of atmospheric CO₂, tropical deforestation alters surface biophysical properties, contributing to decreases in evapotranspiration and surface roughness and increases in albedo when forests are replaced by grasslands and crops^{18–21}. The influence of these biophysical changes has been long appreciated by regional and global climate modeling communities^{22–27} and are known to contribute to regional warming and drying^{28–32}, changes in regional atmospheric circulation and moisture convergence^{33,34}, and longer-range teleconnections^{35–37}. Precipitation responses to tropical deforestation also likely depend on the magnitude and spatial structure of the deforestation pattern. On broader spatial scales, decreases in evapotranspiration may weaken recycling along transport pathways delivering moisture to tropical forests from ocean source regions^{38,39}. At a finer spatial scale, if deforestation contributes to a heterogeneous distribution of surface roughness and atmospheric heating, rainfall may increase in cleared areas and downwind of deforestation patches^{40,41}.

Contrasting climate responses to deforestation across different tropical continents have been found in model simulations^{30,42,43} and are summarized in a recent review³². Studies using climate models agree generally that Amazonian deforestation has the strongest climate impacts, causing regional warming and decreases in precipitation. The regional climate response to deforestation in tropical Africa and Southeast Asia is weaker in magnitude, likely as a consequence of different forms of land-cover change, different climate baseline states, spatial patterns of deforestation, and geographical differences in topography and proximity of forests to nearby ocean regions⁴⁴. For instance, the higher precipitation sensitivity to local surface drying in the Amazon, as compared to other tropical continents, has been recently attributed to different contributions of local evaporative recycling to precipitation in the baseline climate⁴⁵.

An important question when considering the net impact of deforestation on the Earth system is whether deforestation-induced changes in regional climate influence the local environment for remaining forests, making it either easier or more difficult for these forests to grow. Forest loss that causes regional warming and drying, for example, has the potential to contribute to positive carbon–climate feedback because higher air temperatures may reduce photosynthesis^{46,47} and increase autotrophic respiration, leading to lower levels of net primary production and forest cover in nearby areas. Warming and drying also promote drought and wildfire^{15,48}, which greatly increases the risk of regional forest dieback and the associated loss of the aboveground

biomass⁴⁹. An ensuing climate-tipping point, once triggered, may cause local ecosystems to move toward an alternate stable state^{5,32,50,51}, in which grass plant functional types are dominant, wildfires are prevalent, and carbon stocks are considerably reduced. Negative feedback, in contrast, may occur if loss of forest cover contributes to changes in atmospheric circulation that increase regional rainfall⁴⁰ or diffuse light⁵². While previous studies have explored deforestation edge effects^{53,54} on carbon storage in nearby patches from changes in canopy microclimate and fire risk, much less work has examined the carbon consequences of regional-to-continental-scale changes in climate. To determine the magnitude and sign of these larger-scale interactions, here we quantify the influence of deforestation-driven climate change on the carbon storage of forests across different tropical continents. This is important because natural climate solutions are gaining attention as a possible mechanism to slow climate warming. In forest carbon offset programs, a critical need is to provide an accurate estimate of the carbon and climate benefits of a land management action (e.g., avoided deforestation), thus enabling a more effective valuation of the carbon credits issued for a specific project.

In this work, we estimate the biophysical impacts of deforestation on aboveground vegetation carbon stocks by combining deforestation-induced changes in annual mean rainfall and air temperature derived from an idealized global deforestation experiment (deforest–globe) that is part of the Land Use Model Intercomparison Project (LUMIP⁵⁵) of phase 6 of Coupled Model Intercomparison Project (CMIP6), with empirical relationships between climate and aboveground biomass storage derived from contemporary satellite observations. Our analysis compares the relative magnitude of the biophysical carbon cost to the direct aboveground biomass loss from tropical deforestation across three different continental regions (Amazon, Congo, and the maritime continent in tropical Asia). We define the biophysical carbon cost as the additional loss of carbon driven by deforestation-induced climate change. We also report the carbon–climate feedback parameter, gamma (defined as the cumulative carbon loss at each location for a 1°C increase in surface air temperature)⁵⁶ driven solely by the biophysical climate effect of tropical deforestation and compare it to more traditional estimates of gamma derived from radiative effects of increasing CO₂.

Results

Deforestation impacts on tropical climate across continents.

The multimodel mean estimates (obtained from eight fully coupled Earth system models, ESMs^{57–64}, Table 1) of the tropical climate response (Fig. 1) to idealized deforestation (Supplementary Fig. 1) show that many areas across the tropics experience warming and reduced rainfall in response to deforestation. Decreases in rainfall occur across almost all of the Amazon, in the western half of the Congo basin and across the southern part of Borneo and the interior western part of New Guinea (Fig. 1a–c and Supplementary Fig. 2). These reductions are consistent with widespread declines in evapotranspiration in deforested areas, as shown by Boysen et al.⁶⁵, and are partly offset by precipitation increases in northern and eastern Africa. The largest decline of mean annual precipitation occurs in Amazonia, where a $59.0 \pm 16.9\%$ loss in biomass drives a significant precipitation decrease of $150 \pm 105 \text{ mm yr}^{-1}$ ($6.7 \pm 4.7\%$), averaged across all eight models (Table 2). Precipitation reductions for the Congo and for the maritime continent (that is, islands in tropical Southeast Asia) are smaller in relative magnitude, with biomass losses of $50.8 \pm 13.9\%$ and $42.0 \pm 10.2\%$ resulting in mean annual precipitation decreases of $41 \pm 56 \text{ mm yr}^{-1}$ ($2.7 \pm 3.7\%$) and

Table 1 A list of information of 8 Earth system models participating in the LUMIP idealized deforestation experiment.				
Model name	Model center	Original resolution	Dynamic vegetation	Reference
BCC-CSM2-MR	Beijing Climate Center, China	320 × 160 (1.125° × 1.125°)	No	Wu et al. ⁵⁷
CanESM5	Canadian Centre for Climate Modelling and Analysis, Canada	128 × 64 (2.8° × 2.8°)	No	Swart et al. ⁵⁸
CESM2	National Center for Atmospheric Research, USA	288 × 192 (1.25° × 0.94°)	No	Danabasoglu et al. ⁵⁹
CNRM-ESM2-1	Centre National de Recherches Météorologiques, France	256 × 128 (1.4° × 1.4°)	No	Séférian et al. ⁶⁰
IPSL-CM6A-LR	Institut Pierre-Simon Laplace, France	144 × 143 (2.5° × 1.27°)	No	Boucher et al. ⁶¹
GISS-E2-1-G	NASA Goddard Institute for Space Studies, USA	144 × 90 (2.5° × 2°)	No	Kelley et al. ⁶²
UKESM1-0-LL	Met Office Hadley Centre, UK	192 × 144 (1.87° × 1.25°)	Yes	Sellar et al. ⁶³
MPI-ESM1-2-LR	Max Planck Institute for Meteorology, Germany	192 × 96 (1.9° × 1.9°)	No	Mauritsen et al. ⁶⁴

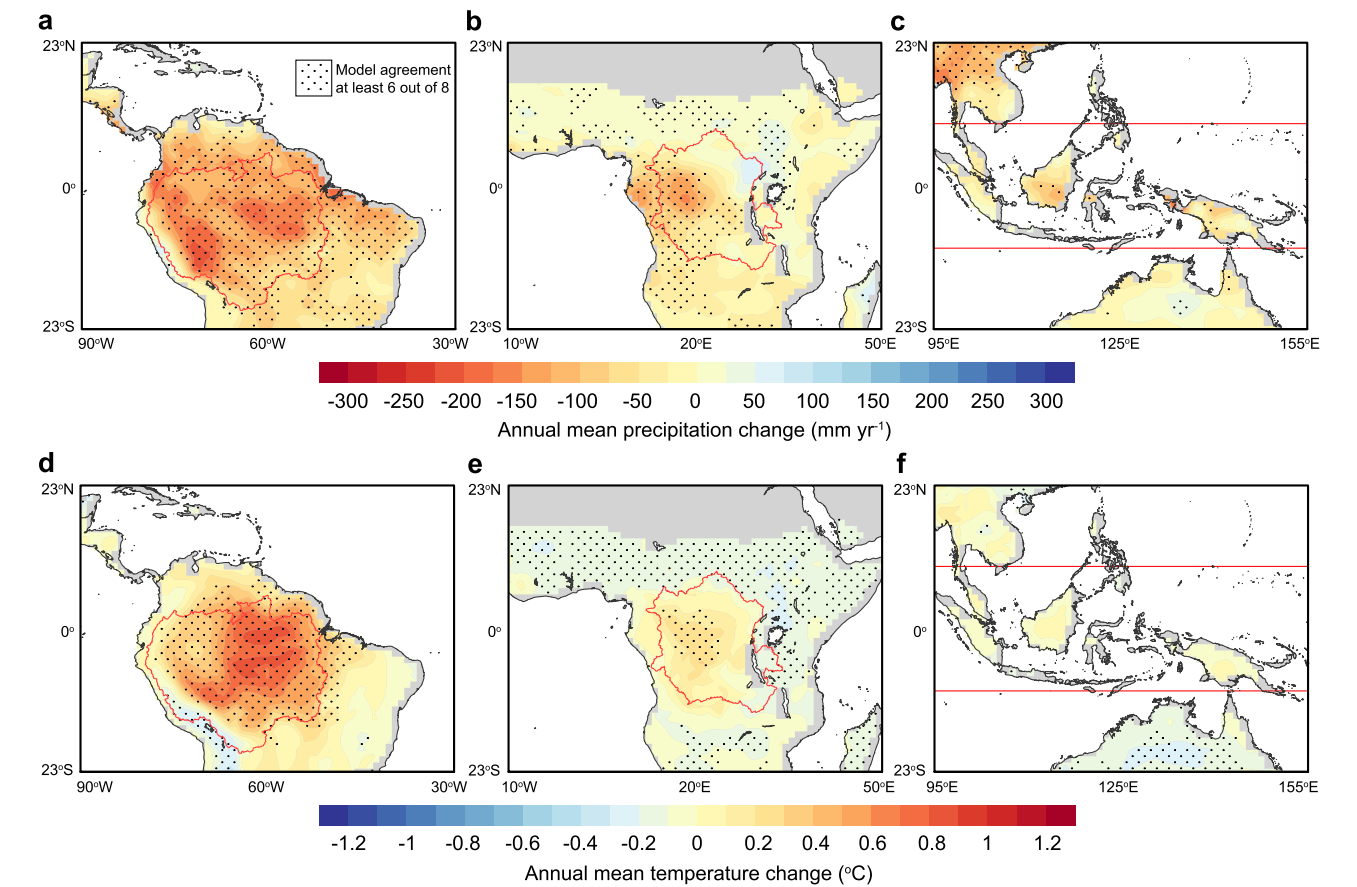


Fig. 1 Biophysical impacts of idealized deforestation on rainfall and temperature in three tropical regions. Changes in mean annual rainfall and air temperature in **a, d**, South America, **(b, e)**, Africa and **(c, f)**, Southeast Asia. The changes were computed as the difference between the average of last 30 years from the LUMIP deforest-globe and piControl experiments (see “Methods”). The dotted area indicates the model agreement, with at least six out of eight models agreeing on the sign of the climate responses. Information on the eight models is listed in Table 1.

$38 \pm 58 \text{ mm yr}^{-1}$ ($1.3 \pm 2.0\%$), for the Congo and the maritime continent, respectively. Model agreement with respect to the direction of the precipitation response to deforestation is high in South America, with at least six of the eight models showing decreases in precipitation across most of the Amazon. Model agreement is lower in the eastern part of the Congo and across tropical Asia, where the magnitude of the multimodel mean change is also smaller relative to background precipitation levels. In response to idealized deforestation, mean annual air temperature increases significantly in the Amazon by $0.5 \pm 0.5^\circ\text{C}$ for the multimodel mean, with smaller and more variable cross-model responses in the Congo ($0.1 \pm 0.5^\circ\text{C}$) and tropical Asia ($-0.1 \pm 0.2^\circ\text{C}$) (Fig. 1d–f and Table 2). The continental differences in the mean annual temperature response

have long been recognized from early climate model simulations of tropical deforestation³⁰ and are explained by tradeoffs between declining surface net radiation (which causes cooling) and reductions in evapotranspiration and surface roughness (which causes surface warming). In the Amazon, latent heat decreases by $6.9 \pm 3.5 \text{ W m}^{-2}$ from deforestation whereas net surface radiation declines by $4.6 \pm 2.5 \text{ W m}^{-2}$ (Supplementary Table 1). In contrast, the latent heat declines by $3.4 \pm 4.5 \text{ W m}^{-2}$ and $2.1 \pm 3.8 \text{ W m}^{-2}$ for the Congo and the islands of tropical Asia, respectively, relative to declines in net radiation of $3.3 \pm 2.9 \text{ W m}^{-2}$ and $1.4 \pm 1.9 \text{ W m}^{-2}$. The weaker warming response in the Congo may be driven by a smaller cloud response (that is, a smaller decrease in cloud cover, Supplementary Fig. 3) in Africa where the diurnal temperature range changes by a

Table 2 Impacts of idealized deforestation on climate and aboveground biomass (AGB) in the tropics ^a .							
Region	Tree cover change (%)	Forest biomass change (%)	Relative precipitation change (%)	Precipitation change ^c (mm yr ⁻¹)	Temperature change (°C)	Total forest AGB loss ^d (Mg C ha ⁻¹)	Estimated AGB loss from the biophysical feedback (Mg C ha ⁻¹)
Amazon ^b	-44.7 (6.0)	-59.0 (16.9)	-6.7 (4.7)	-150 (105)	0.5 (0.5)	-98.3 (13.2)	-5.0 (3.6)
Congo	-38.7 (8.8)	-50.8 (13.9)	-2.7 (3.7)	-41 (56)	0.1 (0.5)	-75.5 (16.7)	-2.9 (1.9)
Tropical Asia	-31.2 (8.9)	-42.0 (10.2)	-1.3 (2.0)	-38 (58)	-0.1 (0.2)	-62.4 (17.8)	-0.3 (2.0)

^aIn parentheses, we present 1 standard deviation (SD) of the mean across models, with the uncertainty of biophysical AGB loss propagated from that of the precipitation and temperature using the equation for observations in Table 3.

^bAmazon and Congo are defined as land grids within the basin map, and tropical Asia is defined as the land grid cells within 10°S–10°N, 95°E–155°E.

^cPrecipitation change was computed as the product between multimodel average relative rainfall change (%) and climatological rainfall observations at each continent, to avoid the influence of simulated rainfall bias on the deforestation impacts on rainfall for each model.

^dTotal forest carbon loss was estimated as the product between the tree cover change in LUMIP deforest-glob simulations after 50 years and the observational tree cover-aboveground biomass relationship as shown in Supplementary Fig. 7.

smaller amount as shown by previous simulations^{36,43}. An asymmetric cloud response between the Amazon and the Congo is seen in ESMs such as CanESM5, CESM2, MPI-ESM-1.2.0, and UKESM1-0-LL, as shown in Supplementary Fig. S6 in ref. ⁶⁵. The smaller latent heat decline for the tropical Asian islands is expected since climatological precipitation is much larger than in the other two regions, which means that evaporation is less frequently water-limited. Further, the temperature over the maritime continent is more tightly controlled by the surrounding ocean.

The sensitivity of tropical aboveground biomass to climate. To assess the response of tropical aboveground vegetation carbon storage to the biophysical climate effects of deforestation, we developed an empirical relationship between tropical aboveground biomass (AGB) from the ESA-CCI BIOMASS project³ and climate observations (see “Methods”), drawing upon the spatial variability of biomass and climate across different tropical regions (Fig. 2a). We used all resampled 1-degree grid cells within 23°S–23°N (including forests and grasses) in our analysis except for desert regions with mean annual precipitation less than 100 mm yr⁻¹ and grid cells with a land fraction less than 50%. Across the tropics, drier areas also have more spatial variation in mean annual temperature, with lower AGB observed in regions with higher mean annual temperature (Fig. 2a). Both the Congo and the Amazon are closer to a 1500 mm yr⁻¹ threshold that separates tropical forests and savannas⁶⁶, suggesting forests in these regions are closer to a climate-tipping point. The climate-AGB relationship derived from the spatial variation in observations reflects the long-term evolutionary and adaptive responses of the terrestrial ecosystem to climate, and implicitly includes processes such as fires, deforestation and drought effects on tree mortality⁶⁶. The CMIP6 multimodel mean captures the general spatial sensitivity of AGB to precipitation and temperature variations (Fig. 2b) despite the simulated AGB by models are biased a bit low in areas with a high fraction of forests (Supplementary Fig. 4).

We first used a multiple linear regression model to estimate the AGB sensitivity to the spatial variations in temperature and precipitation, with the aim of combining this information with the climate impacts of deforestation to estimate the biophysical feedback effect of deforestation on AGB. Table 3 shows that observed mean annual temperature and mean annual precipitation explain 49% of the spatial variance in tropical AGB using the climate and biomass observations, with the AGB increasing by 3.4 Mg C ha⁻¹ for 100 mm yr⁻¹ increase in precipitation (8.2% per 100 mm yr⁻¹). Similarly, AGB declines by 0.32 Mg C ha⁻¹ for every 1 °C increase in mean annual temperature (-0.8% per °C) (Table 3). This larger AGB sensitivity to precipitation is in contrast to a recent report⁴⁷ that finds that the tropical forest AGB is more sensitive to maximum temperature (-5.9% per °C) rather than rainfall (2.4% per 100 mm yr⁻¹). When comparing our findings to those in the previous study, it is important to note our regression is also derived from non-forest biomes in the tropics, including savannas and grasslands (Supplementary Fig. 5). Therefore, the climate gradient that we consider is larger, and rainfall therefore has a more significant role in defining the transition from forests to savannas.

To tailor a climate-biomass statistical model for use in wetter areas where tropical forests are dominant, we used a moving window on climatological annual rainfall (see “Methods”). This analysis indicates that tropical AGB rainfall sensitivity is the largest between 1500 mm yr⁻¹ and 2000 mm yr⁻¹ (Fig. 2c), collocated with the average rainfall climatology in the Congo basin and the southern and eastern parts of the Amazon. This

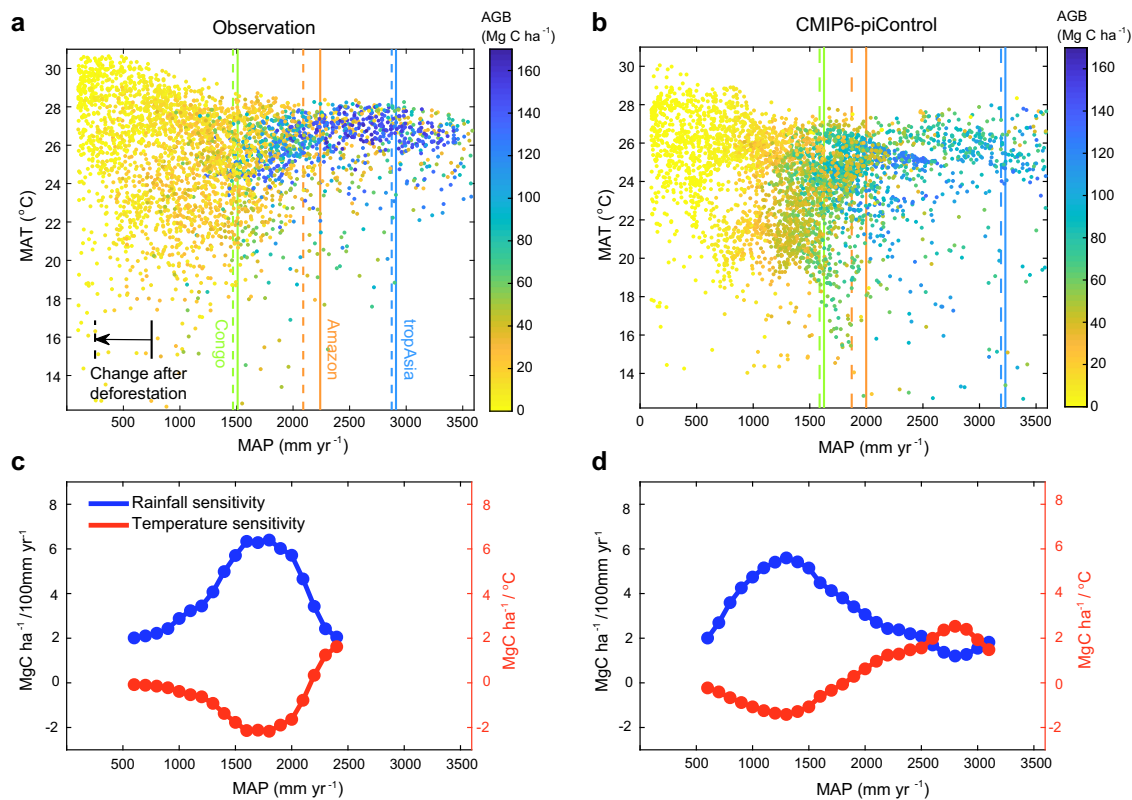


Fig. 2 Aboveground biomass (AGB) relationships with mean annual temperature (MAT) and precipitation (MAP) derived from both observations and CMIP6 models. **a, b** AGB from satellite data (ESA-CCI) and from CMIP6-piControl experiment averaged in climate space of MAT and MAP. AGB from CMIP6 was computed from the total vegetation carbon multiplied by a mean ratio between the aboveground and total biomass weighted by the tree cover fraction (see “Methods”). **c, d** Statistical sensitivity of AGB to MAP and MAT for observation-based data and CMIP6 simulations, respectively. The sensitivity of AGB to MAP and MAT was estimated from a regression within each moving window spanning $\pm 500 \text{ mm yr}^{-1}$ and centered at each MAP level from 600 to 3100 mm yr^{-1} . The dotted curves indicate the range over which the regressions were significant at $P < 0.001$. No significant relationships were found for the observations above a MAP of 2400 mm yr^{-1} . Vertical lines in panels a and b represent mean precipitation levels for each region before (solid) and after (dashed) the deforestation.

Table 3 Overview of the statistical model of observed and simulated aboveground biomass (AGB) in relation to mean annual precipitation (MAP) and temperature (MAT).						
	a*100	b	R ²	RMSE	δ_{MAP}	δ_{MAT}
Observations ^a	3.4	−0.32	0.49	32 Mg C ha ^{−1}	8.2% /100 mm yr ^{−1}	−0.8%/°C
CMIP6 mean	3.2	−0.04	0.60	23 Mg C ha ^{−1}	6.9% /100 mm yr ^{−1}	−0.09%/°C

^aEquation: $\text{AGB} = a \cdot \text{MAP} + b \cdot \text{MAT} + \varepsilon$. The units are mm yr^{-1} for MAP, °C for MAT, and Mg C ha^{-1} for AGB. δ_{MAP} and δ_{MAT} indicate the relative AGB sensitivity to MAP and MAT (in percentage), computed as the relative value of the coefficients a and b to the observed/simulated AGB averaged for the whole tropical region. RMSE denotes the root mean square error.

suggests that the aboveground vegetation carbon storage is more sensitive to rainfall changes in tropical Africa and South America than in tropical Asia. An AGB spatial sensitivity analysis with two other satellite AGB products^{1,2} shows consistent results to those derived with the ESA-CCI product (Supplementary Fig. 6). Within the CMIP6 models, the multiple linear regression explains 60% of the spatial variability in AGB (Table 3). The sensitivity of AGB to precipitation within the CMIP6 models is similar to the observations (6.9% per 100 mm yr^{−1}) but the temperature sensitivity is considerably lower (−0.1 % per °C) (Fig. 2b, d). We also explored the impact of other or more specific environmental factors such as vapor pressure deficit (VPD), mean annual maximum temperature, the seasonality of temperature and precipitation, and precipitation during the driest three months (see “Methods”). These metrics are thought to be physiologically meaningful for tropical forest growth^{47,67}.

We found that these physiological environment factors have a high spatial collinearity with the mean annual temperature and precipitation (“Methods”) and, therefore, their capability to explain the spatial variation of observed AGB and simulated aboveground vegetation carbon is comparable to that of mean annual temperature and mean annual precipitation (Supplementary Tables 2 and 3). Consequently, for simplicity, we used the AGB sensitivity solely to mean annual temperature and mean annual precipitation (Fig. 2c) to quantify the impacts of deforestation-induced changes in regional climate on tropical AGB.

AGB costs of deforestation-driven changes in climate. To estimate the carbon costs of deforestation-driven changes in surface biophysics, we combined the climate changes from the LUMIP idealized deforestation experiment (Fig. 1) with the

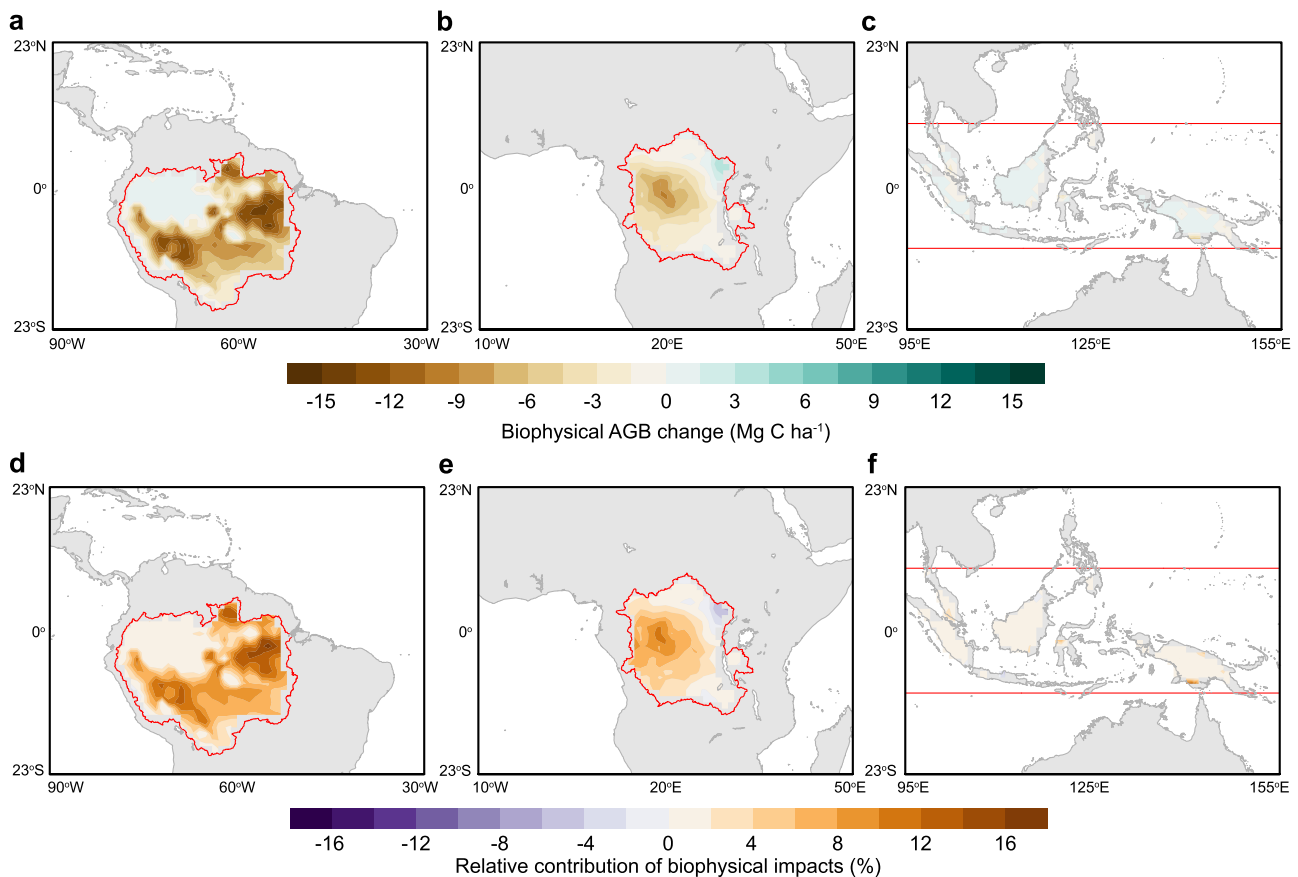


Fig. 3 Biophysical impacts of deforestation on aboveground biomass (AGB) in the tropics. **a–c** Shows biophysical AGB changes of deforestation estimated from the product of deforestation-induced changes in climate (mean annual precipitation and mean annual temperature), and the observational sensitivity of the AGB to precipitation and temperature shown in Fig. 2c. **d–f** Shows the relative change of (**a–c**) as a percent of the estimated direct AGB loss from deforestation (see “Methods”).

moving window climate–AGB relationship we derived from the observations (Fig. 2c). Warming and drying from deforestation contributed to an AGB loss of $5.0 \pm 3.6 \text{ Mg C ha}^{-1}$ in the Amazon, $2.9 \pm 1.9 \text{ Mg C ha}^{-1}$ in the Congo, and $0.3 \pm 2.0 \text{ Mg C ha}^{-1}$ for the islands in tropical Asia (Table 2). The satellite observations indicate that AGB decreases by about $19\text{--}22 \text{ Mg C ha}^{-1}$ per 10% decrease in tree cover fraction in the tropics (Supplementary Fig. 7). Using this relationship derived from the observations and the tree cover fraction changes from the LUMIP models, we estimated that the direct AGB carbon losses due to deforestation in the idealized deforestation experiments are $98.3 \pm 13.2 \text{ Mg C ha}^{-1}$, $75.5 \pm 16.7 \text{ Mg C ha}^{-1}$, and $62.4 \pm 17.8 \text{ Mg C ha}^{-1}$ in the Amazon, Congo, and tropical Asia, respectively (Table 2). These estimated AGB carbon losses are larger than that simulated explicitly in the ESM simulations (Supplementary Fig. 1) as the model simulations of the aboveground vegetation carbon stocks are smaller than the satellite observations due in part to a lower atmospheric CO_2 level in the preindustrial era (Supplementary Fig. 4). Expressed relative to the direct AGB loss in the deforestation experiment, the biophysical effects of deforestation contribute to $5.1 \pm 3.7\%$ (that is, $(-5.0 \pm 3.6 \text{ Mg C ha}^{-1})/(-98.3 \text{ Mg C ha}^{-1})$) of additional AGB loss in the Amazon, $3.8 \pm 2.5\%$ of additional loss in the Congo, and $0.5 \pm 3.2\%$ in tropical Asia.

Figure 3 shows the spatial pattern of the biophysical effects of deforestation on AGB and their percent contribution to total biomass loss related to the direct effects of deforestation. Despite the widespread decline in rainfall and warming, the largest AGB

loss due to biophysical feedback occurs in the eastern Amazon where the additional AGB loss is as high as 14 Mg C ha^{-1} (17%) (Fig. 3a, d). There is no additional AGB loss predicted for the northwestern Amazon due to its high baseline precipitation level that reduces the sensitivity of AGB to changes in precipitation or temperature (Fig. 2c). Biophysical effects also amplify the AGB loss in the central Congo Basin by up to 9 Mg C ha^{-1} (11%) but do not lead to any additional AGB loss in tropical Asia as a consequence of its high precipitation baseline (Fig. 3b, c, e, f). Further separation of the effects of deforestation-driven changes in temperature and precipitation indicates that it is the precipitation response that controls the spatial pattern of the biophysical carbon costs (Fig. 4), highlighting the importance of water stress in regulating tropical deforestation-driven AGB changes.

By applying the relationship that we obtained from LUMIP simulations and the satellite AGB observations, we can estimate the influence of past deforestation during the historical era on regional climate and the associated additional carbon losses. For South America, the mean primary forest fraction declined by 11.5% in the Amazon basin from 1850 to 2015, according to the Land Use Harmonization (LUHv2h) dataset⁶⁸. Using the information from the LUMIP simulations, this decline would translate into a regional precipitation decrease of about 38.6 mm yr^{-1} and a temperature increase of about 0.13°C . Multiplied by the observed AGB–climate sensitivity (Fig. 2c), these biophysical climate effects (mainly from rainfall reduction) associated with deforestation would be equivalent to an additional

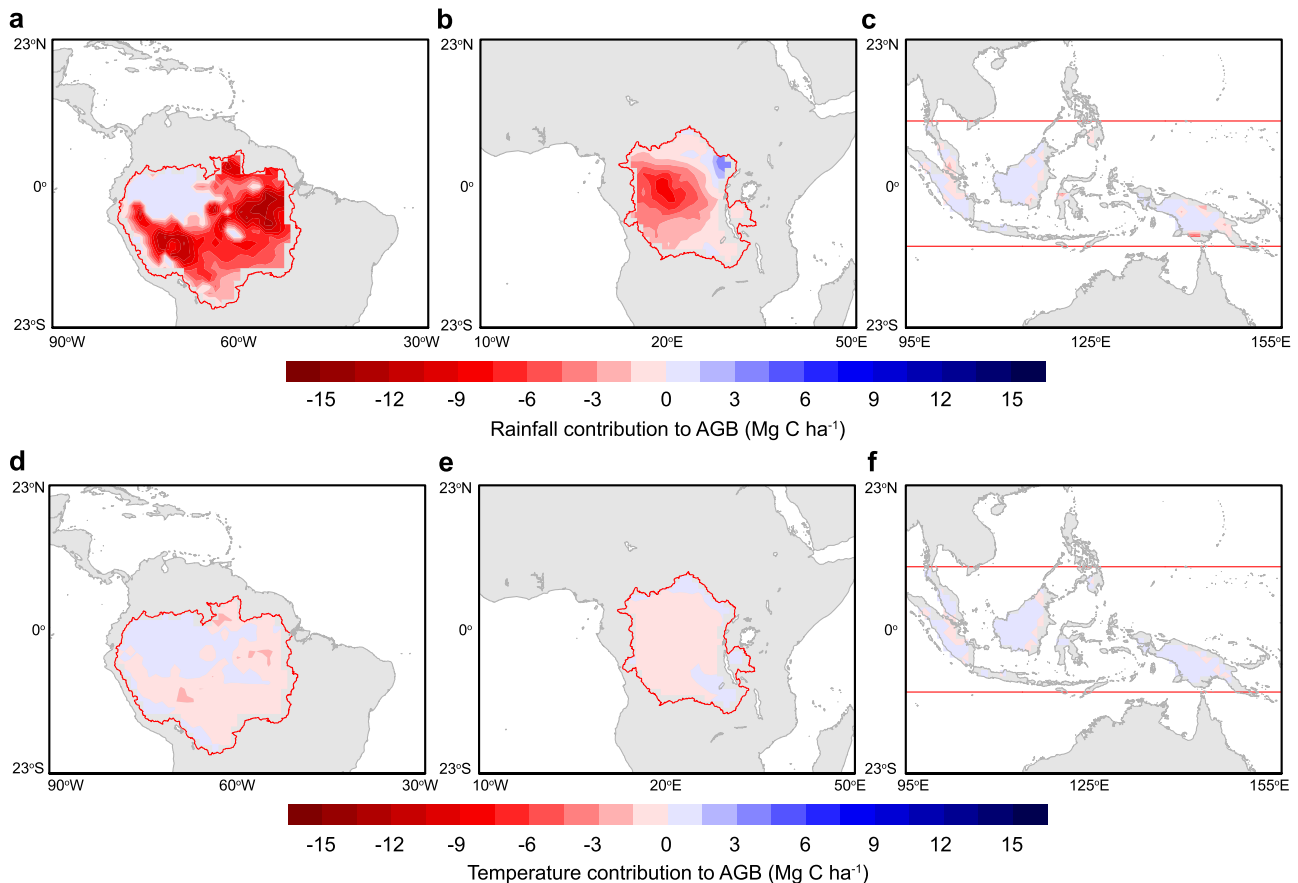


Fig. 4 Contribution of rainfall and air temperature change to the total biophysical aboveground biomass (AGB) loss associated with deforestation. **a–c** Shows precipitation contributions to the biophysical AGB costs of deforestation across the three different tropical regions. **d–f** Shows temperature contributions to the biophysical AGB costs of deforestation. The partitioning is based on results shown in Fig. 3a–c but separates the contributions from the deforestation-induced change in annual mean precipitation and temperature. The relative contribution of precipitation change to biophysical AGB loss varies from 80 to 100% in the Amazon and from 85 to 100% in the Congo.

AGB loss of 741 Tg C (Supplementary Table 4). In Africa, 8.4% loss in primary forest fraction was estimated to cause regional reduction in rainfall by 8.8 mm yr^{-1} and warming by 0.02°C , resulting in a cumulative biophysical AGB loss of about 200 Tg C from 1850 to 2015 (Supplementary Table 4).

Deforestation-driven climate–carbon cycle feedback parameter.

Climate warming is projected in CMIP5 and CMIP6 models to reduce tropical land carbon storage, which is described by a γ parameter that is often negative in sign for tropical terrestrial ecosystems (see Fig. 6.22 in refs. ⁶⁹ and ⁷⁰). Here we estimated γ from the LUMIP models by combining deforestation-driven temperature and carbon stock changes and compare this estimate of γ (i.e., $\gamma_{\text{AGB}}^{\text{def,biophys}}$, see “Methods”) with estimates derived from CO_2 -driven climate change (i.e., $\gamma_{\text{AGB}}^{\text{CO}_2}$, see “Methods”) for the same set of CMIP6 models. Similar to previous conclusions regarding the response of land carbon storage to climate change⁶⁹, we find that the most negative $\gamma_{\text{AGB}}^{\text{CO}_2}$ is in the Amazon, with smaller magnitude of $\gamma_{\text{AGB}}^{\text{CO}_2}$ values in the Congo and across the islands in tropical Asia (Fig. 5a–c). It should be noted that this $\gamma_{\text{AGB}}^{\text{CO}_2}$ calculation does not account for any biophysical climate effects of land use and land-cover change⁷¹. We apply a similar approach to calculate a new deforestation-driven climate–carbon feedback parameter $\gamma_{\text{AGB}}^{\text{def,biophys}}$ by normalizing the biophysical carbon costs of tropical deforestation by the deforestation-caused warming (see “Methods”). Figure 5d–f show that the $\gamma_{\text{AGB}}^{\text{def,biophys}}$ is, in general,

more than twofold higher than the $\gamma_{\text{AGB}}^{\text{CO}_2}$ derived from the idealized CO_2 increasing experiments in the Amazon and Congo. This is because the biophysical effects of deforestation influence the aboveground vegetation carbon mainly through a regionally concentrated rainfall response, with the temperature response being much smaller. Our analysis on the biophysical carbon costs of tropical deforestation, therefore, suggests that the positive carbon–climate feedback from deforestation is fundamentally larger than the feedback originating from fossil emissions.

Discussion

Our analysis indicates that the biophysical climate effects of tropical deforestation, particularly as a consequence of precipitation reductions, add to committed carbon emissions by an extra $5.1 \pm 3.7\%$ in the Amazon and by an extra $3.8 \pm 2.5\%$ in Congo. The additional carbon losses occur as a consequence of remaining intact forests experiencing hotter and drier conditions that reduce carbon storage in aboveground biomass. These findings suggest that the value of avoided deforestation and forest degradation may be underestimated if current carbon assessment methodologies focus only on the direct carbon stock and emission changes associated with the land-use change^{72,73}. The biophysical additionality identified here should be complementary to other co-benefits, including the potential of remaining forests to serve as a future terrestrial carbon sink in response to rising levels of atmospheric carbon dioxide and other global change drivers^{74,75}. The regional differences in the deforestation biophysical changes

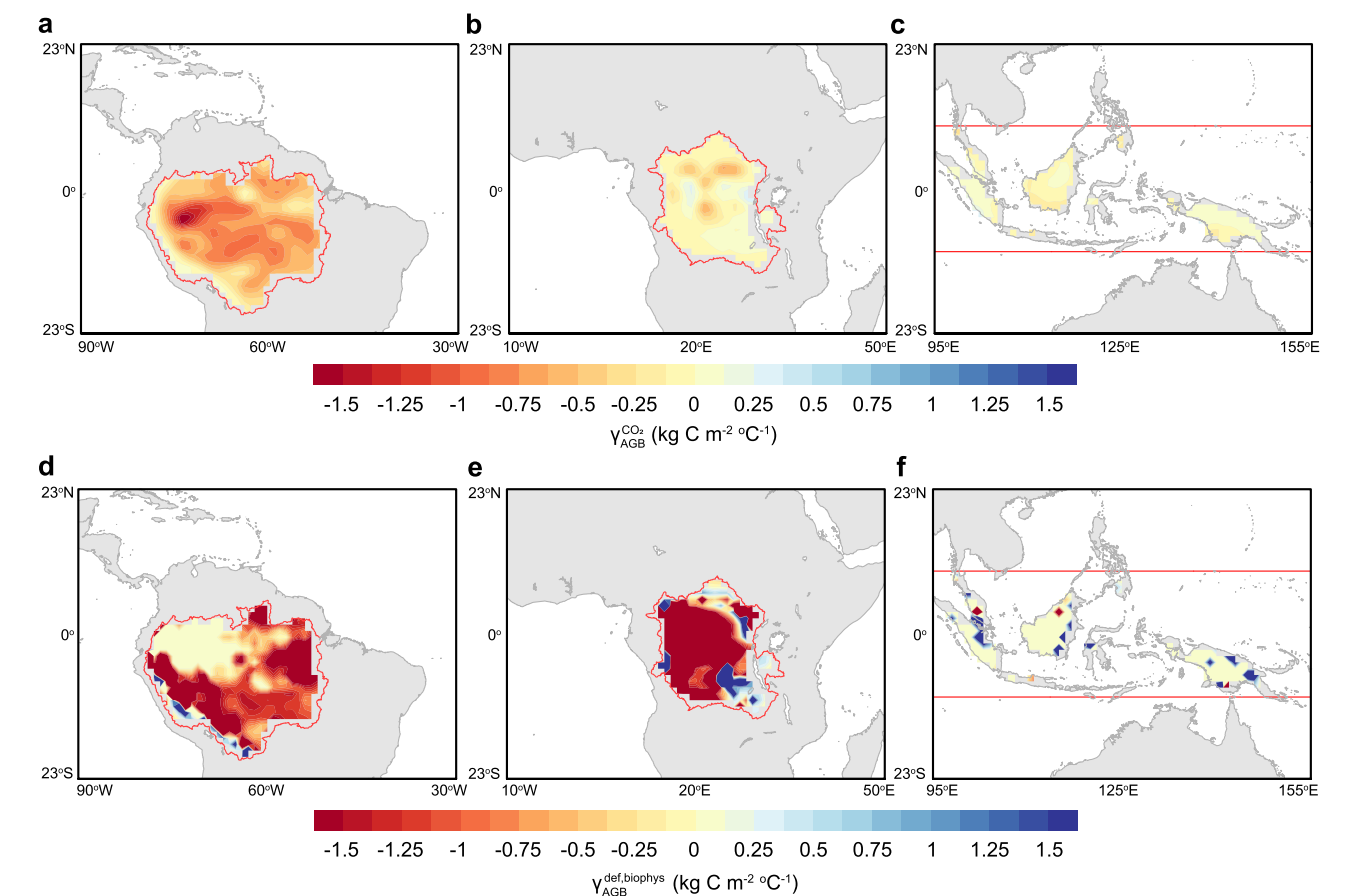


Fig. 5 Spatial pattern of the CO₂-driven and deforestation-driven carbon-climate feedback parameters. **a–c** Shows the climate–AGB feedback parameter (γ) from an idealized increasing of $\sim 4 \times \text{CO}_2$ experiments ($\gamma_{AGB}^{CO_2}$), and **d–f** shows the same quantity derived from the climate change derived from the LUMIP deforestation experiment and associated AGB losses ($\gamma_{AGB}^{def,biophys}$). $\gamma_{AGB}^{CO_2}$ was computed as the difference of changes in AGB between the full and biogeochemical transient CO₂ increasing experiments normalized by warming under the full coupled warming as the following ref.⁷⁰. $\gamma_{AGB}^{def,biophys}$ was computed as the ratio of the deforestation-driven climate impacts on the AGB relative to the deforestation-induced climate warming (see “Methods”).

Table 4 Additional benefits for avoiding deforestation or reforestation associated with the indirect local and regional effects of deforestation on aboveground biomass (AGB).			
Mechanism	Impact of edge or climate feedback on AGB		Citation
	Mean	Range	
Local edge effects (from changes in microclimate and fire)	36% (Amazon) ^a	25–56%	Junior et al. ⁵⁴ Zhao et al. ⁷⁷ Ordway and Asner ⁷⁸
	19% (Congo) ^b	18–20%	
	10% (Tropical Asia) ^c	7–13%	
Regional climate feedback (from changes in rainfall and temperature)	5.1% (Amazon)	1.4–8.8%	This study
	3.8% (Congo)	1.3–6.3%	
	0.5% (Tropical Asia)	0.0–3.7%	
Local edge + regional climate feedback	41% (Amazon)	26–65%	
	23% (Congo)	19–26%	
	11% (Tropical Asia)	7–17%	

^aRatio between total gross carbon loss from edge effect and that from deforestation during 2001–2015.
^bRatio between carbon loss from edge effect and that from deforestation for scenarios 1–3 under the Representative Concentration Pathway 8.5 (RCP8.5) for the entire continent of Africa.
^cRatio of biomass loss has been reported to range from 16 to 30% according to forest sites observations in Sabah, Malaysian Borneo⁷⁸. This ratio has been multiplied by an average fraction of forest fragmentation of 31% (Fischer et al.⁷⁹), and further divided by the remaining forest fraction of 69% that could experience potential large-scale deforestation.

in forest carbon stocks that we uncover may also provide insight about a more equitable approach for assigning carbon credits in the context of Reducing Emissions from Deforestation and forest Degradation projects (REDD+) (e.g., ref. ⁷⁶) and other climate policy frameworks. An important next step in this context is to combine the deforestation biophysical climate effect identified here with AGB losses associated with local edge effects^{54,77–79} in order to estimate an integrated indirect carbon benefit associated with avoided deforestation (or reforestation) projects in the tropics. A preliminary comparison of these two mechanisms and their total effects are provided in Table 4. In the Amazon, these indirect benefits of avoided deforestation may sum to be 41% (with a range of 26–65%) higher than carbon contained within the project boundaries.

The positive biophysical climate feedback of tropical deforestation (e.g., warming and reduced precipitation as revealed by previous single model-based studies^{22–27} and our multimodel analysis) has important implications for assessing future climate risks of tropical moist forests^{50,80}. From our analysis of LUMIP–CMIP6 simulations, idealized deforestation by 45% contributes to an Amazonian rainfall decline by $150 \pm 105 \text{ mm yr}^{-1}$, which is comparable to the expected change in rainfall observed in idealized 1% CO_2 physiological effect experiments (that is, by -175 mm yr^{-1} in response to a $4 \times \text{CO}_2$ increase for CMIP5, ref. ⁴⁵). If we presume that these two effects can be linearly combined that would mean a 325 mm yr^{-1} reduction of precipitation for a climatology of about 2240 mm yr^{-1} (Fig. 2). An annual mean precipitation threshold of 1500 mm yr^{-1} has been identified as the typical hydrological boundary between tropical forests and savannas^{66,81}. The total precipitation expected changes from CO_2 physiology and deforestation together suggest that the mean Amazonian precipitation may not cross the hydrological threshold necessary for a permanent transition to a savanna-like state in response to these drivers. However, in southern and eastern areas of the Amazon, where current precipitation levels are much closer to this tipping point, these combined effects may push ecosystems over this threshold and may be further amplified by the direct (radiative) effects of global climate change.

In contrast, deforestation-driven decreases in rainfall in the western Congo and in some areas of tropical Asia may be partially offset by the radiative and physiological effects of rising CO_2 , which may increase precipitation in these regions as a consequence of interactions between surface biophysical changes and regional atmospheric circulation⁴⁵. Nevertheless, the change of mean climate by deforestation (that is, less rainfall and warming), as revealed in our analysis of the LUMIP–CMIP6 simulations, still implies the increasing possibility of a lengthening dry season⁸², an increasing amplitude of extreme drought events⁸³, and a higher likelihood of wildfires^{5,10,15} in the tropics if deforestation continues in the future. More broadly, the high levels of uncertainty regarding how radiative, physiological, and land-cover change mechanisms influence tropical precipitation make it challenging to accurately predict climate-tipping points in the tropics.

The carbon–climate feedback parameter γ was initially proposed to measure the carbon cycle response to climate warming^{56,70}, irrespective of whether the warming originates from fossil fuel emissions or carbon emissions from land-use change. In past applications, γ has been found to be negative (i.e., a loss of carbon to the atmosphere for a 1°C temperature increase) across tropical land ecosystems as a consequence of increases in ecosystem respiration and decreases in photosynthesis caused by warming⁸⁴. As far as we are aware, past work has not estimated γ driven by warming from the biophysical effects of tropical deforestation. This warming is fundamentally different because it is associated with large changes in precipitation and other land surface variables in the tropics, including humidity and wind speed. Here, we find that the deforestation-driven $\gamma_{\text{AGB}}^{\text{def, biophys}}$ (i.e., the term considering the biophysical warming effect of deforestation on the carbon cycle in the tropics) could be twofold larger in the Amazon and Congo than that computed from the idealized CO_2 increasing experiment without consideration of land-use and land-cover change ($\gamma_{\text{AGB}}^{\text{CO}_2}$, as derived from the Coupled Climate–Carbon Cycle Model Intercomparison Project experiments (C4MIP) for CMIP6, ref. ⁷¹). This implies that the warming caused by biophysical effects of tropical deforestation has stronger impacts on nearby tropical terrestrial ecosystems than warming originating from global radiative

forcing of the Earth system, once adjusted for the same change in temperature. Further analysis on the attribution of future tropical climate change to deforestation and CO_2 is needed for a better understanding of the role of tropical land use and land cover in the climate system. In future work, higher resolution model simulations may help to identify optimal locations for forest restoration efforts in order to offset precipitation declines from historic deforestation and maximize climate change mitigation from tropical reforestation efforts.

There are several key uncertainties associated with tropical deforestation and its biophysical impact on precipitation and temperature including whether or not precipitation and temperature are linearly or nonlinearly dependent on the amount of deforestation, masking of the precipitation response by internal climate variability, and the potential for the deforestation-driven climate changes to impact fires and therefore to feedback onto aboveground vegetation carbon stocks by means of changes in the disturbance regime. Further work is needed to explore nonlinearities in the carbon costs of tropical forest loss and the drivers of continental-scale differences. Experiments and analysis using high-resolution models could help refine the cloud and convection responses to deforestation. More research on local and remote teleconnections is also needed. Specifically, more work is needed by the Earth system community to understand how deforestation or reforestation in different regions (on individual continents) influence local and remote patterns of precipitation³⁸ and other aspects of near-surface climate. This may include further effort to develop a process-based evaluation framework for quantifying the impact of deforestation on regional climate that reconciles predictions from ESMs with long-term trends from satellites and field observations, building on the framework developed by Duveiller et al.⁸⁵ for evaluating the influence of vegetation cover on surface energy exchange. Additional improvements of ESMs to better represent forest mortality, convection, and precipitation in tropical climate simulations also would help us more accurately assess the carbon costs of deforestation and evaluate their role in the changing climate system.

Our study provides a means to estimate the additional carbon losses associated with the regional to continental-scale biophysical effects of deforestation and their impact on regional climate and the carbon stocks of nearby undisturbed forests. For the Amazon, avoiding deforestation provides an additional $5.1 \pm 3.7\%$ benefit for aboveground vegetation carbon storage based on the model-simulated deforestation–climate effects and climate–vegetation carbon relationships derived from observations. For the Congo, this additionality is $3.8 \pm 2.5\%$. We find that such biophysical carbon costs of deforestation mainly arise from regional declines in precipitation and are further amplified by increases in surface air temperature. This, in combination with the estimated strong deforestation-driven climate–vegetation carbon feedback, emphasizes the additional threat from regional water stress triggered by deforestation and the potential effectiveness of climate mitigation strategies that maintain or expand robust tropical forest ecosystems.

Methods

CMIP6 simulations. Precipitation, surface air temperature, vegetation carbon (being converted to the carbon in the aboveground biomass, AGB, using an empirical factor, that is, 0.8 for forests and 0.4 for savannas, see below), and tree cover fraction from 8 available Earth system models (ESMs^{57–64}) (Table 1) participating in the Land Use Model Intercomparison Project (LUMIP) with model participating in phase 6 of Coupled Model Intercomparison Project (CMIP6)⁵⁵ were used in this study. The idealized deforestation simulations (deforest-glob) from LUMIP assume that a total forest area of 20 million km^2 was linearly removed from the top 30% of forested area across the globe in 50 years. After 50 years, deforestation activity stopped, and most models were run for another

30 years for the purpose of reaching a stable status. The idealized global deforestation experiments caused a significant decline in tropical tree cover fraction, with the multimodel mean tree cover fraction decreasing by $44.7 \pm 6.0\%$, $38.7 \pm 8.8\%$ and $31.2 \pm 8.9\%$ in Amazon, Congo, and islands in tropical Asia, respectively (Table 2).

The above-mentioned variables from the preindustrial control (piControl) simulations of the eight models that participated in the LUMIP deforestation experiments were used to provide a referenced climate background in the tropics. This is justified by the fact that the LUMIP deforestation simulations start from a boundary condition that is identical to that in the piControl simulations. The first realization (r1) was selected for all 8 models for both the deforest-globe and piControl simulations, except for CESM2, for which the second realization (r2) in the deforest-globe simulations were selected due to a shifted rainfall climatology in r1.

We also downloaded these variables of the above 8 ESMs participating in the Coupled Climate–Carbon Cycle Model Intercomparison Project (C4MIP)⁷¹, to calculate the CO₂-driven climate–vegetation carbon feedback parameter (detailed approach is described in detail below). The C4MIP experiments contain simulations of the idealized 1% per year increasing CO₂ experiments (1pctCO₂), with the capability of CO₂ separately influencing the radiation components (1pctCO₂-rad) and the carbon cycle model components (1pctCO₂-bgc). These factorial experiment designs enable the isolation of the climate–carbon cycle feedback parameter (that is, the sensitivity of a carbon pool to climate warming, γ ⁶⁹, with a unit of $\text{kg C m}^{-2} \text{ } ^\circ\text{C}^{-1}$). γ was computed by subtracting the land carbon storage in 1pctCO₂-bgc simulations from the 1pctCO₂ simulations and by dividing this term by the corresponding climate warming in the 1pctCO₂ simulations. In C4MIP experiments, 1pctCO₂, 1pctCO₂-rad, and 1pctCO₂-bgc were run for each model for 140 years under a transient CO₂ increasing at a rate of 1% per year. By the end of 140 years, the atmospheric CO₂ concentration quadruples to about 1120 ppm. We thus represented the $4 \times \text{CO}_2$ effects on climate and aboveground vegetation carbon by computing their difference between the last and first 20-year averages for each 140-yr simulation in 1pctCO₂ and 1pctCO₂-bgc simulations. All variables from the above experiments were remapped to the 1-degree grid using the bilinear interpolation method from Climate Data Operator (CDO)⁸⁶.

Observations. Contemporary observations of mean annual precipitation and surface air temperature, derived from the Tropical Rainfall Measuring Mission (TRMM⁸⁷) and Climate Research Unit (CRU TS4.04, ref. ⁸⁸), were used to obtain the empirical relationship between climate and the AGB. The observational AGB (unit: Mg ha^{-1} , being converted to Mg C ha^{-1} using a factor of 0.5, ref. ⁸⁹) was derived from the European Space Agency Climate Change Initiative (ESA–CCI) BIOMASS project³. ESA–CCI biomass map provides detailed information of the aboveground vegetation carbon storage during the year 2010, 2017, 2018 at a spatial resolution of $100 \times 100 \text{ m}$. In this study, we used the AGB map during the year of 2017. The accuracy of ESA–CCI AGB has been improved when compared to the previous version (that is, AGB from GlobBiomass project, used in land surface model evaluation⁸⁹), with the upper limit of AGB relative error being 20% where AGB exceeds 50 Mg ha^{-1} and a fixed error of 10 Mg ha^{-1} where the AGB is below that limit (see Product Validation & Algorithm Selection Report Version 2 in <https://climate.esa.int/en/projects/biomass/key-documents/>). Nevertheless, ESA–CCI may still underestimate AGB in wet tropics because both L- and C-band backscatter data saturate at high AGB levels when AGB values keep increasing. We averaged the original AGB data to a $1^\circ \times 1^\circ$ grid, corresponding to the unified resolution of the LUMIP model output used in this study. Accordingly, observed satellite precipitation from TRMM and air temperature from CRU in the year of 2017 were downloaded and aggregated to the same 1-degree resolution.

Other observational data include AGB data from ref. ¹ and ref. ², land cover from the Moderate Resolution Imaging Spectroradiometer (MODIS) data (MCD 12C1, distinguishing the land fraction within each 1-degree pixel), and MODIS vegetation continuous fields (VCF) data (MOD44B, used as the observational tree cover fraction as shown in Supplementary Fig. 7) during the year of 2017. We also used the observed precipitation from Global Precipitation Climatology Centre (GPCC)⁹⁰ and estimated climatological (1987–2016 average) precipitation in the Amazon, Congo, and tropical Asia (Supplementary Table 4).

Deforestation effects on rainfall and temperature. For each model, the deforestation impacts on mean annual precipitation and temperature were computed as the difference of the last 30-year average between the deforest-glob and the piControl simulations. For the multimodel mean, we calculated the agreement of these eight models on the sign of the deforestation-caused change in precipitation and temperature, with at least six out of eight models agreement indicated by the dotted area shown in Fig. 1. A recent study by Boysen et al.⁶⁵ has given an overview of the simulated deforestation effects on global climate. Although tropical rainfall and air temperature may be perturbed significantly by deforestation in the extratropical regions (in particular, see remote effects by high-latitude deforestation in Devaraju et al.²⁶), most models agree that deforestation causes an averaged warming and decline in rainfall due to the large-scale decline in evapotranspiration within the tropics⁶⁵.

To confirm that most of the tropical climate response originates from tropical deforestation in the LUMIP experiments, we conducted an additional experiment

with CESM2. This experiment exactly followed the LUMIP protocol⁵⁵ but excluded deforestation in the extratropics poleward of 23°S – 23°N . We ran the model for 80 years, with tropical tree cover losses exactly equivalent to those in CESM2 participating in the LUMIP deforest-glob experiments. Different from the LUMIP deforest-glob simulations, in this experiment (CESM-trop) all tree cover fraction was invariant in the extratropics. To eliminate the influence from model version or initial conditions, we ran the same model in a configuration of the preindustrial conditions for another 30 years (CESM2-ctl). The difference in precipitation and temperature over the last 30 years between CESM2-trop and CESM2-ctl thus represents the climate effects of deforestation only in the tropics in CESM2. This experiment confirmed that most of the simulated changes in precipitation and temperature over tropical forests originated from deforestation within the tropics. Nevertheless, more work is needed to systematically examine tropical and extratropical deforestation contributions (e.g., remote effects on tropical monsoon precipitation by high-latitude deforestation via shifting the intertropical convergence zone²⁶) to regional climate across the full suite of CMIP models.

Spatial AGB sensitivity to rainfall and air temperature. To obtain the climate sensitivity of the aboveground biomass (AGB), we first applied a multiple linear regression model to the observational or simulated grids of biomass as a function of the mean annual precipitation (MAP) and temperature (MAT) across the tropics (23°S – 23°N) (Table 3).

$$\text{AGB} = a * \text{MAP} + b * \text{MAT} + \varepsilon \quad (1)$$

The regression was applied to all land grids in the observational datasets (see above descriptions) for the year of 2017 within 23°S – 23°N , excluding those with a MAP lower than 100 mm yr^{-1} and land fraction lower than 0.5 (mainly the edge pixels on islands in tropical Asia). The land fraction was computed using MCD12C1 land cover. The coefficients of a and b were shown in Table 3 for both the observations and CMIP6 mean.

Despite using all land grid cells in the regression method, we found that the AGB spatial sensitivity varies as a function of climatological mean rainfall (Fig. 2c). We thus applied the regression method to estimate the AGB–climate sensitivity at different precipitation levels. Each level of precipitation (that is, from 600 to 3100 mm yr^{-1} at an interval of 100 mm yr^{-1}) is the center rainfall condition of each moving window spanning $\pm 500 \text{ mm yr}^{-1}$ (for example, land grid cells with precipitation from 100 mm yr^{-1} to 1100 mm yr^{-1} were used in the regression for estimating AGB–climate sensitivity at the precipitation level of 600 mm yr^{-1}) (Fig. 2c). This approach was also used to estimate the subsequent AGB costs of tropical deforestation impacts through changing the regional climate.

Observational climate sensitivity of the AGB may be influenced by spatial variation in contemporary disturbance regimes, including fire and agriculture, which were not considered in the piControl simulations of the models. To test the robustness of the regression-derived parameters in the observations, we applied a similar multiple linear regression model to the simulated AGB and precipitation, and temperature from the piControl simulations of LUMIP models. On basis of previously identified empirical ratios for aboveground to total biomass (that is, 0.8 for forests and 0.4 for savannas⁹¹), LUMIP ESMs simulated total vegetation carbon was multiplied by a mean factor weighted by the simulated tree cover fraction (that is, mean factor = $0.8 \times \text{tree cover} + 0.4 \times (1 - \text{tree cover})$) and converted to AGB carbon.

An implicit assumption here is that aboveground vegetation carbon in the tropics is influenced by the precipitation- and temperature-induced changes in environmental factors (including the subsequent changes in soil moisture and the vapor pressure deficit, VPD), which influences aboveground vegetation carbon through changes in vegetation physiological processes (for example, stomatal closure). We also computed the observed VPD, mean annual maximum temperature (MAXT), the seasonality of precipitation (P_{amp} , defined as the difference in rainfall between the month with the maximum value and the month with the minimum value), the seasonality of temperature (T_{amp} , defined as the difference in temperature between the month with the maximum value and the month with the minimum value), and precipitation in the driest quarter (PRD, defined as the minimum rainfall of consecutive 3 months throughout the year). We diagnosed the relationship of these metrics with MAT and MAP using the Belsley collinearity diagnostics using the software MATLAB. We found that T_{amp} , MAXT, and VPD have high spatial collinearity with the MAT, while P_{amp} and PRD have high spatial collinearity with the MAP. Models with these extra variables did not significantly improve the goodness of fit of the regression model (Supplementary Tables 2 and 3). This suggests that these water and heat stress factors that are critical for plant physiological processes covary spatially to a high degree with the mean annual precipitation and surface air temperature.

Biophysical AGB loss from tropical deforestation. We estimated the biophysical AGB costs of tropical deforestation (Fig. 3a–c) by multiplying the deforestation-induced climate change from LUMIP (Fig. 1) and the observed AGB carbon sensitivity to mean annual precipitation and air temperature (Fig. 2c). We focused on three tropical continents (Amazon, Congo, and islands in tropical Asia) with a high fraction of intact forests where the signal of deforestation–climate impacts is also relatively robust (Fig. 1). Instead of using a unified AGB sensitivity to MAP and MAT (shown in Table 3), we used the moving window AGB–climate

sensitivity at different rainfall levels to estimate the carbon costs of tropical deforestation-driven climate change as the AGB-climate sensitivity varies with the rainfall background (Fig. 2c). When applying this moving window approach, we inferred the AGB-climate sensitivity at each grid cell by its background rainfall level, which was computed as the GPCC⁹⁰ climatological precipitation average plus the deforestation-induced change in relative rainfall (%) from the LUMIP experiments. To measure the relative role of these biophysically driven carbon losses, we first estimated the direct AGB losses due to losses of the multimodel mean tree cover in LUMIP. The LUMIP ESMs simulated AGB loss along with deforestation cannot represent the realistic values as the ESMs have a negative bias for AGB in tropical regions with high fraction of forests (Supplementary Fig. 4). To estimate the realistic direct AGB loss due to deforestation, we used the observational relationship between AGB and tree cover fraction, both of which were derived from the satellite observations. Supplementary Fig. 7 shows that a 10% loss in tree cover fraction corresponds to 19–22 Mg C ha⁻¹ loss in AGB for the observations. Using this ratio in three tropical regions, combined with the multimodel mean tree cover loss, we estimated that the tree cover losses by 44.7 ± 6.0%, 38.7 ± 8.8%, and 31.2 ± 8.9% in LUMIP corresponds to direct AGB carbon losses by -98.3 ± 13.2 Mg C ha⁻¹, -75.5 ± 16.7 Mg C ha⁻¹, and -62.4 ± 17.8 Mg C ha⁻¹ in the Amazon, Congo, and maritime continent in tropical Asia, respectively (Table 2). The relative role of biophysical carbon costs of tropical deforestation was calculated as the ratio of the biophysically driven AGB loss to the estimated direct AGB losses (Table 2 and Fig. 3d–f).

By assuming the ESM-diagnosed deforestation-climate relationships are a linear function of the deforestation level⁹², we estimated the cumulative impacts of past deforestation on regional climate and carbon stocks. To quantify the past history of deforestation, we used the Land Use Harmonization (LUHv2h) dataset⁶⁸ spanning the period from 1850 to 2015. Considering the Amazon basin, for example, (also see Supplementary Table 4), the mean annual precipitation decline caused by primary forest loss (-11.5%) was estimated to be -1.7%, and the mean annual warming was estimated to be 0.13 °C. Applying the climate sensitivity of AGB (Fig. 2c), this yielded a cumulative AGB loss of 1.3 Mg C ha⁻¹ from rainfall decline and an additional gain of 0.04 Mg C ha⁻¹ from warming. Together, these add up to about 741 Tg C for the Amazon basin (area, 5,840,000 km²). Using the same approach (Supplementary Table 4), we estimated the biophysically driven AGB loss for the Congo to be 200 Tg C 1850 to 2015 from losses in forest cover (Supplementary Table 4).

CO₂- and deforestation-driven climate-vegetation carbon feedback. The CO₂-driven climate-carbon cycle feedback considers the isolation of the land carbon-climate sensitivity, γ , from fully coupled (1pctCO₂) and biogeochemically coupled (1pctCO₂-bgc) idealized climate simulations^{56,69,70}. Here we modified this approach to consider only the contribution to γ arising from changes in AGB at each grid cell (CMIP6 simulated vegetation carbon was converted to the AGB using an empirical factor, that is, 0.8 for forests and 0.4 for savannas):

$$\gamma_{AGB}^{CO_2} = \frac{\Delta C'_{AGB} - \Delta C^*_{AGB}}{\Delta T'} \quad (2)$$

where $\Delta C'_{AGB}$ and ΔC^*_{AGB} represent the changes in the AGB from 1pctCO₂ and 1pctCO₂-bgc simulations, and $\Delta T'$ denotes the increases in surface air temperature from 1pctCO₂. The changes of AGB carbon and air temperature from these two simulations were quantified as the difference between the last and first 20-year average (for both two simulations, 140 years in total). $\gamma_{AGB}^{CO_2}$ thus represents the CO₂-driven climate-carbon feedback parameter (see the first row in Fig. 5).

The CO₂-driven climate-carbon feedback framework considers the biogeochemical climate effects of increased CO₂ concentration that may come from both fossil fuel and land-use change carbon emissions but does not consider the contribution from the land-use physical effect of tropical deforestation, and therefore may underestimate the land-use risk for the carbon-climate feedback in the tropics. Using the LUMIP simulated biophysical deforestation effects and the sensitivity of the AGB to climate derived from the observations, we calculated the deforestation-driven carbon-climate feedback parameter as follows:

$$\gamma_{AGB}^{def, biophys} = \frac{\Delta C_{AGB}^{def, biophys}}{\Delta T^{def, biophys}} \quad (3)$$

where $\gamma_{AGB}^{def, biophys}$ denote the climate sensitivity of the AGB carbon under tropical deforestation. $\Delta C_{AGB}^{def, biophys}$ and $\Delta T^{def, biophys}$ represent the biophysical effects of deforestation on tropical AGB carbon and air temperature, respectively. $\Delta T^{def, biophys}$ was computed as the LUMIP models simulated air temperature change in the tropics, while $\Delta C_{AGB}^{def, biophys}$ was calculated as the sum of the deforestation-caused changes in mean annual precipitation and temperature, multiplied by the observational AGB sensitivity to precipitation and temperature, respectively. $\gamma_{AGB}^{CO_2}$ and $\gamma_{AGB}^{def, biophys}$ are shown in the first and second row of Fig. 5, respectively.

Data availability

All CMIP6 simulations are publicly available via <https://esgf-node.llnl.gov/projects/cmip6/>. Observational precipitation from TRMM 3B43 and climate variables from CRU TS4.04 are accessible via the websites: https://disc.gsfc.nasa.gov/datasets/TRMM_3B43_7/

https://crudata.uea.ac.uk/cru/data/hrg/cru_ts_4.04/, respectively. ESA-CCI AGB is available via: <https://climate.esa.int/en/projects/biomass/>. AGB from ref. ¹ is available via: <https://www.ilamb.org/ILAMB-Data/DATA/biomass/Tropical/>. AGB from ref. ² is available via: https://developers.google.com/earth-engine/datasets/catalog/WHRC_biomass_tropical. MODIS MCD12C1 and MOD44B are available via EarthData: <https://earthdata.nasa.gov/>. Processed data for this study have been deposited in Li Yue: (2022). Data supporting figures of deforestation_carbon_biophysics (v1.0). Zenodo. <https://doi.org/10.5281/zenodo.6326365>.

Code availability

Code and scripts of CESM2 can be downloaded through the website via: https://escomp.github.io/CESM2/versions/cesm2.1/html/downloading_cesm.html. Scripts for all figures and tables are at https://github.com/YueLi92/deforestation_carbon_biophysics, which has been deposited in Li, Yue: (2022). Code supporting deforestation_carbon_biophysics (v1.0). Zenodo. <https://doi.org/10.5281/zenodo.6323730>.

Received: 5 August 2021; Accepted: 23 March 2022;

Published online: 12 April 2022

References

1. Saatchi, S. S. et al. Benchmark map of forest carbon stocks in tropical regions across three continents. *Proc. Natl. Acad. Sci. USA* **108**, 9899–9904 (2011).
2. Baccini, A. et al. Estimated carbon dioxide emissions from tropical deforestation improved by carbon-density maps. *Nat. Clim. Chang* **2**, 182–185 (2012).
3. Santoro, M. et al. The global forest above-ground biomass pool for 2010 estimated from high-resolution satellite observations. *Earth Syst. Sci. Data* **13**, 3927–3950 (2021).
4. Cox, P. M. et al. Sensitivity of tropical carbon to climate change constrained by carbon dioxide variability. *Nature* **494**, 341–344 (2013).
5. Davidson, E. A. et al. The Amazon basin in transition. *Nature* **481**, 321–328 (2012).
6. Ramankutty, N. & Foley, J. A. Estimating historical changes in global land cover: croplands from 1700 to 1992. *Glob. Biogeochem. Cy.* **13**, 997–1027 (1999).
7. Pongratz, J., Reick, C., Raddatz, T. & Claussen, M. A reconstruction of global agricultural areas and land cover for the last millennium. *Glob. Biogeochem. Cy.* **22**, GB3018 (2008).
8. Kaplan, J. O. et al. Holocene carbon emissions as a result of anthropogenic land cover change. *Holocene* **21**, 775–791 (2011).
9. Fearnside, P. M. Deforestation in Brazilian Amazonia: history, rates, and consequences. *Conserv. Biol.* **19**, 680–688 (2005).
10. van Marle, M. J. et al. Fire and deforestation dynamics in Amazonia (1973–2014). *Glob. Biogeochem. Cy.* **31**, 24–38 (2017).
11. Houghton, R. A. & Nassikas, A. A. Global and regional fluxes of carbon from land use and land cover change 1850–2015. *Glob. Biogeochem. Cy.* **31**, 456–472 (2017).
12. Houghton, R. A. Aboveground forest biomass and the global carbon balance. *Glob. Change Biol.* **11**, 945–958 (2005).
13. Friedlingstein, P. et al. Global carbon budget 2020. *Earth Syst. Sci. Data* **12**, 3269–3340 (2020).
14. Xu, L. et al. Changes in global terrestrial live biomass over the 21st century. *Sci. Adv.* **7**, eaab9829 (2021).
15. Brando, P. M. et al. The gathering firestorm in southern Amazonia. *Sci. Adv.* **6**, eaay1632 (2020).
16. Qin, Y. et al. Carbon loss from forest degradation exceeds that from deforestation in the Brazilian Amazon. *Nat. Clim. Chang.* **11**, 442–448 (2021).
17. Erb, K. H. et al. Unexpectedly large impact of forest management and grazing on global vegetation biomass. *Nature* **553**, 73–76 (2018).
18. Bonan, G. B. Forests and climate change: forcings, feedbacks, and the climate benefits of forests. *Science* **320**, 1444–1449 (2008).
19. Davin, E. L. & de Noblet-Ducoudré, N. Climatic impact of global-scale deforestation: radiative versus nonradiative processes. *J. Clim.* **23**, 97–112 (2010).
20. Li, Y. et al. Local cooling and warming effects of forests based on satellite observations. *Nat. Commun.* **6**, 1–8 (2015).
21. Silvério, D. V. et al. Agricultural expansion dominates climate changes in southeastern Amazonia: the overlooked non-GHG forcing. *Environ. Res. Lett.* **10**, 104015 (2015).
22. Betts, R. Implications of land ecosystem-atmosphere interactions for strategies for climate change adaptation and mitigation. *Tellus Ser. B-Chem. Phys. Meteorol.* **59**, 602–615 (2007).
23. Gibbard, S., Caldeira, K., Bala, G., Phillips, T. J. & Wickett, M. Climate effects of global land cover change. *Geophys. Res. Lett.* **32**, L23705 (2005).

24. Bala, G. et al. Combined climate and carbon-cycle effects of large-scale deforestation. *Proc. Natl Acad. Sci. USA* **104**, 6550–6555 (2007).
25. Bathiany, S., Claussen, M., Brovkin, V., Raddatz, T. & Gayler, V. Combined biogeophysical and biogeochemical effects of large-scale forest cover changes in the MPI earth system model. *Biogeosciences* **7**, 1383–1399 (2010).
26. Devaraju, N., Bala, G. & Modak, A. Effects of large-scale deforestation on precipitation in the monsoon regions: Remote versus local effects. *Proc. Natl Acad. Sci. USA* **112**, 3257–3262 (2015).
27. Devaraju, N., Bala, G. & Nemani, R. Modelling the influence of land-use changes on biophysical and biochemical interactions at regional and global scales. *Plant Cell Environ.* **38**, 1931–1946 (2015).
28. Henderson-Sellers, A. & Gornitz, V. Possible climatic impacts of land cover transformations, with particular emphasis on tropical deforestation. *Clim. Change* **6**, 231–257 (1984).
29. Dickinson, R. E. & Henderson-Sellers, A. Modelling tropical deforestation: a study of GCM land-surface parametrizations. *Q. J. R. Meteorol. Soc.* **114**, 439–462 (1988).
30. Zhang, H., Henderson-Sellers, A. & McGuffie, K. Impacts of tropical deforestation. Part I: process analysis of local climatic change. *J. Clim.* **9**, 1497–1517 (1996).
31. Costa, M. H. & Foley, J. A. Combined effects of deforestation and doubled atmospheric CO₂ concentrations on the climate of Amazonia. *J. Clim.* **13**, 18–34 (2000).
32. Lawrence, D. & Vandecar, K. Effects of tropical deforestation on climate and agriculture. *Nat. Clim. Chang.* **5**, 27–36 (2015).
33. Nobre, C. A., Sellers, P. J. & Shukla, J. Amazonian deforestation and regional climate change. *J. Clim.* **4**, 957–988 (1991).
34. Gedney, N. & Valdes, P. J. The effect of Amazonian deforestation on the northern hemisphere circulation and climate. *Geophys. Res. Lett.* **27**, 3053–3056 (2000).
35. Nobre, P., Malagutti, M., Urbano, D. F., de Almeida, R. A. & Giarolla, E. Amazon deforestation and climate change in a coupled model simulation. *J. Clim.* **22**, 5686–5697 (2009).
36. Snyder, P. K. The influence of tropical deforestation on the Northern Hemisphere climate by atmospheric teleconnections. *Earth Interact.* **14**, 1–34 (2010).
37. Spracklen, D. V., Baker, J. C. A., Garcia-Carreras, L. & Marsham, J. H. The effects of tropical vegetation on rainfall. *Annu. Rev. Environ. Resour.* **43**, 193–218 (2018).
38. Leite-Filho, A. T., Soares-Filho, B. S., Davis, J. L., Abrahão, G. M. & Börner, J. Deforestation reduces rainfall and agricultural revenues in the Brazilian Amazon. *Nat. Commun.* **12**, 1–7 (2021).
39. Baidya Roy, S. & Avissar, R. Impact of land use/land cover change on regional hydrometeorology in Amazonia. *J. Geophys. Res. Atmos.* **107**, LBA-4 (2002).
40. Khanna, J., Medvigy, D., Fisch, G. & de Araújo Tiburtino Neves, T. T. Regional hydroclimatic variability due to contemporary deforestation in southern Amazonia and associated boundary layer characteristics. *J. Geophys. Res. Atmos.* **123**, 3993–4014 (2018).
41. McGuffie, K., Henderson-Sellers, A., Zhang, H., Durbidge, T. B. & Pitman, A. J. Global climate sensitivity to tropical deforestation. *Glob. Planet. Change* **10**, 97–128 (1995).
42. Zhang, H., Henderson-Sellers, A. & McGuffie, K. The compounding effects of tropical deforestation and greenhouse warming on climate. *Clim. Change* **49**, 309–338 (2001).
43. Voldoire, A. & Royer, J. F. Climate sensitivity to tropical land surface changes with coupled versus prescribed SSTs. *Clim. Dyn.* **24**, 843–862 (2005).
44. Mahmood, R. et al. Land cover changes and their biogeophysical effects on climate. *Int. J. Climatol.* **34**, 929–953 (2014).
45. Kooperman, G. J. et al. Forest response to rising CO₂ drives zonally asymmetric rainfall change over tropical land. *Nat. Clim. Chang.* **8**, 434–440 (2018).
46. Doughty, C. E. & Goulden, M. L. Are tropical forests near a high temperature threshold? *J. Geophys. Res. Biogeosci.* **113**, G00B07 (2008).
47. Sullivan, M. J. et al. Long-term thermal sensitivity of Earth's tropical forests. *Science* **368**, 869–874 (2020).
48. Wu, C. et al. Historical and future global burned area with changing climate and human demography. *One Earth* **4**, 517–530 (2021).
49. Brando, P. M. et al. Abrupt increases in Amazonian tree mortality due to drought–fire interactions. *Proc. Natl Acad. Sci. USA* **111**, 6347–6352 (2014).
50. Nobre, C. A. et al. Land-use and climate change risks in the Amazon and the need of a novel sustainable development paradigm. *Proc. Natl Acad. Sci. USA* **113**, 10759–10768 (2016).
51. Trumbore, S., Brando, P. & Hartmann, H. Forest health and global change. *Science* **349**, 814–818 (2015).
52. Green, J. K., Berry, J., Ciais, P., Zhang, Y. & Gentile, P. Amazon rainforest photosynthesis increases in response to atmospheric dryness. *Sci. Adv.* **6**, eabb7232 (2020).
53. Numata, I. et al. Biomass collapse and carbon emissions from forest fragmentation in the Brazilian Amazon. *J. Geophys. Res. Biogeosci.* **115**, G03027 (2010).
54. Junior, C. H. S. et al. Persistent collapse of biomass in Amazonian forest edges following deforestation leads to unaccounted carbon losses. *Sci. Adv.* **6**, eaaz8360 (2020).
55. Lawrence, D. M. et al. The Land Use Model Intercomparison Project (LUMIP) contribution to CMIP6: rationale and experimental design. *Geosci. Model Dev.* **9**, 2973–2998 (2016).
56. Friedlingstein, P. et al. Climate–carbon cycle feedback analysis: results from the C4MIP model intercomparison. *J. Clim.* **19**, 3337–3353 (2006).
57. Wu, T. et al. The Beijing Climate Center climate system model (BCC-CSM): the main progress from CMIP5 to CMIP6. *Geosci. Model Dev.* **12**, 1573–1600 (2019).
58. Swart, N. C. et al. The Canadian Earth System Model version 5 (CanESM5.0.3). *Geosci. Model Dev.* **12**, 4823–4873 (2019).
59. Danabasoglu, G. et al. The Community Earth System Model version 2 (CESM2). *J. Adv. Model Earth Syst.* **12**, e2019MS001916 (2020).
60. Séférian, R. et al. Evaluation of CNRM Earth System Model, CNRM-ESM2-1: role of earth system processes in present-day and future climate. *J. Adv. Model Earth Syst.* **11**, 4182–4227 (2019).
61. Boucher, O. et al. Presentation and evaluation of the IPSL-CM6A-LR climate model. *J. Adv. Model Earth Syst.* **12**, 1–52 (2020).
62. Kelley, M. et al. GISS-E2. 1: configurations and climatology. *J. Adv. Model Earth Syst.* **12**, e2019MS002025 (2020).
63. Sellar, A. A. et al. Implementation of UK Earth system models for CMIP6. *J. Adv. Model Earth Syst.* **12**, e2019MS001946 (2020).
64. Mauritsen, T. et al. Developments in the MPI-M Earth System Model version 1.2 (MPI-ESM1. 2) and its response to increasing CO₂. *J. Adv. Model Earth Syst.* **11**, 998–1038 (2019).
65. Boysen, L. et al. Global climate response to idealized deforestation in CMIP6 models. *Biogeosciences* **17**, 5615–5638 (2020).
66. Malhi, Y. et al. Exploring the likelihood and mechanism of a climate-change-induced dieback of the Amazon rainforest. *Proc. Natl Acad. Sci. USA* **106**, 20610–20615 (2009).
67. Novick, K. A. et al. The increasing importance of atmospheric demand for ecosystem water and carbon fluxes. *Nat. Clim. Chang.* **6**, 1023–1027 (2016).
68. Hurtt, G. C. et al. Harmonization of global land use change and management for the period 850–2100 (LUH2) for CMIP6. *Geosci. Model Dev.* **13**, 5425–5464 (2020).
69. Ciais, P. et al. Carbon and other biogeochemical cycles. In *Climate Change 2013: The Physical Science Basis. Contribution of Working Group I to the Fifth Assessment Report of the Intergovernmental Panel on Climate Change*. (eds Stocker et al.) 465–570 (Cambridge Univ Press, UK and USA, 2013).
70. Arora, V. K. et al. Carbon–concentration and carbon–climate feedbacks in CMIP6 models and their comparison to CMIP5 models. *Biogeosciences* **17**, 4173–4222 (2020).
71. Jones, C. D. et al. C4MIP–The coupled climate–carbon cycle model intercomparison project: experimental protocol for CMIP6. *Geosci. Model Dev.* **9**, 2853–2880 (2016).
72. UNFCCC. Background paper for the Workshop on Reducing Emissions from Deforestation in Developing Countries, Part 1: Scientific, Socio-economic, Technical, and Methodological Issues Related to Deforestation in Developing Countries 30 August to 1 September, Rome, Italy. Working paper No. 1(a) (2006).
73. Asner, G. P. Tropical forest carbon assessment: integrating satellite and airborne mapping approaches. *Environ. Res. Lett.* **4**, 034009 (2009).
74. Mahowald, N. M. et al. Interactions between land use change and carbon cycle feedbacks. *Glob. Biogeochem. Cy* **31**, 96–113 (2017).
75. Hubau, W. et al. Asynchronous carbon sink saturation in African and Amazonian tropical forests. *Nature* **579**, 80–87 (2020).
76. Gibbs, H. K., Brown, S., Niles, J. O. & Foley, J. A. Monitoring and estimating tropical forest carbon stocks: making REDD a reality. *Environ. Res. Lett.* **2**, 045023 (2007).
77. Zhao, Z. et al. Fire enhances forest degradation within forest edge zones in Africa. *Nat. Geosci.* **14**, 479–483 (2021).
78. Ordway, E. M. & Asner, G. P. Carbon declines along tropical forest edges correspond to heterogeneous effects on canopy structure and function. *Proc. Natl Acad. Sci. USA* **117**, 7863–7870 (2020).
79. Fischer, R. et al. Accelerated forest fragmentation leads to critical increase in tropical forest edge area. *Sci. Adv.* **7**, eabg7012 (2021).
80. McDowell, N. et al. Drivers and mechanisms of tree mortality in moist tropical forests. *N. Phytol.* **219**, 851–869 (2018).
81. Staver, A. C., Archibald, S. & Levin, S. A. The global extent and determinants of savanna and forest as alternative biome states. *Science* **334**, 230–232 (2011).
82. Fu, R. et al. Increased dry-season length over southern Amazonia in recent decades and its implication for future climate projection. *Proc. Natl Acad. Sci. USA* **110**, 18110–18115 (2013).

83. Bagley, J. E., Desai, A. R., Harding, K. J., Snyder, P. K. & Foley, J. A. Drought and deforestation: has land cover change influenced recent precipitation extremes in the Amazon? *J. Clim.* **27**, 345–361 (2014).
84. Arora, V. K. et al. Carbon–concentration and carbon–climate feedbacks in CMIP5 Earth system models. *J. Clim.* **26**, 5289–5314 (2013).
85. Duveiller, G. et al. Biophysics and vegetation cover change: a process-based evaluation framework for confronting land surface models with satellite observations. *Earth Syst. Sci. Data* **10**, 1265–1279 (2018).
86. Schulzweida, U. Climate data operators (CDO) user guide (Version 1.9.8). <https://doi.org/10.5281/zenodo.3539275> (2019).
87. Tropical Rainfall Measuring Mission (TRMM) TRMM (TMPA/3B43) Rainfall Estimate L3 1 month 0.25 degree x 0.25 degree V7, Greenbelt, MD, Goddard Earth Sciences Data and Information Services Center (GES DISC). <https://doi.org/10.5067/TRMM/TMPA/MONTH/7> (2011).
88. Harris, I., Osborn, T. J., Jones, P. & Lister, D. Version 4 of the CRU TS monthly high-resolution gridded multivariate climate dataset. *Sci. Data* **7**, 1–18 (2020).
89. Yang, H. et al. Comparison of forest above-ground biomass from dynamic global vegetation models with spatially explicit remotely sensed observation-based estimates. *Glob. Chang. Biol.* **26**, 3997–4012 (2020).
90. Schneider, U. et al. GPCC Full Data Reanalysis Version 6.0 at 1.0°: Monthly Land-Surface Precipitation from Rain-Gauges built on GTS-based and Historic Data. https://doi.org/10.5676/DWD_GPCC/FD_M_V7_100 (2011).
91. Liu, Y. Y. et al. Recent reversal in loss of global terrestrial biomass. *Nat. Clim. Chang* **5**, 470–474 (2015).
92. Spracklen, D. V. & Garcia-Carreras, L. The impact of Amazonian deforestation on Amazon basin rainfall. *Geophys. Res. Lett.* **42**, 9546–9552 (2015).

Acknowledgements

This work was funded by NASA’s SERVIR Amazonia program in the form of a grant (80NSSC20K0590) to D.C.M., P.M.B., and J.T.R., by NASA’s Carbon Monitoring System (CMS) and Modeling, Analysis and Prediction (MAP) programs (80NSSC18K0179), and by the US. Dept. of Energy Office of Science RUBISCO Science Focus Area. D.M.L. is supported by the National Center for Atmospheric Research, which is a major facility sponsored by the NSF under Cooperative Agreement No. 1852977.

Author contributions

Y.L. and J.T.R. designed the research; Y.L. performed data analysis and model simulations; Y.L. and J.T.R. drafted the manuscript, with discussions and contributions from P.M.B., D.C.M., D.M.L., and H.Y.; All authors reviewed and revised the manuscript.

Competing interests

The authors declare no competing interests.

Additional information

Supplementary information The online version contains supplementary material available at <https://doi.org/10.1038/s41467-022-29601-0>.

Correspondence and requests for materials should be addressed to Yue Li.

Peer review information *Nature Communications* thanks the anonymous reviewer(s) for their contribution to the peer review of this work. Peer reviewer reports are available.

Reprints and permission information is available at <http://www.nature.com/reprints>

Publisher’s note Springer Nature remains neutral with regard to jurisdictional claims in published maps and institutional affiliations.



Open Access This article is licensed under a Creative Commons Attribution 4.0 International License, which permits use, sharing, adaptation, distribution and reproduction in any medium or format, as long as you give appropriate credit to the original author(s) and the source, provide a link to the Creative Commons license, and indicate if changes were made. The images or other third party material in this article are included in the article’s Creative Commons license, unless indicated otherwise in a credit line to the material. If material is not included in the article’s Creative Commons license and your intended use is not permitted by statutory regulation or exceeds the permitted use, you will need to obtain permission directly from the copyright holder. To view a copy of this license, visit <http://creativecommons.org/licenses/by/4.0/>.

© The Author(s) 2022